THE JOURNAL OF BIOLOGICAL CHEMISTRY VOL. 292, NO. 4, pp. 1145–1159, January 27, 2017

The Chemical Basis of Thiol Addition to Nitro-conjugated Linoleic Acid, a Protective Cell-signaling Lipid*[S]◆

Received for publication, August 30, 2016, and in revised form, November 23, 2016 Published, JBC Papers in Press, December 6, 2016, DOI 10.1074/jbc.M116.756288

Lucía Turell[‡§1,2], Darío A. Vitturi[¶1], E. Laura Coitiño[‖2], Lourdes Lebrato[‡§], Matías N. Möller[§2], Camila Sagasti[‖], Sonia R. Salvatore[¶], Steven R. Woodcock[¶], Beatriz Alvarez[‡§2,3], and Francisco J. Schopfer[¶4]**

*From the Laboratorios de ‡Enzimología, ‖Química Teórica y Computacional, and **Fisicoquímica Biológica, Instituto de Química Biológica, Facultad de Ciencias, and §Center for Free Radical and Biomedical Research, Universidad de la República, Montevideo 11400, Uruguay and the ¶Department of Pharmacology and Chemical Biology, University of Pittsburgh School of Medicine, Pittsburgh, Pennsylvania 15213*

Edited by F. Peter Guengerich

Nitroalkene fatty acids are formed *in vivo* and exert protective and anti-inflammatory effects via reversible Michael addition to thiol-containing proteins in key signaling pathways. Nitro-conjugated linoleic acid (NO_2-CLA) is preferentially formed, constitutes the most abundant nitrated fatty acid in humans, and contains two carbons that could potentially react with thiols, modulating signaling actions and levels. In this work, we examined the reactions of NO_2-CLA with low molecular weight thiols (glutathione, cysteine, homocysteine, cysteinylglycine, and β-mercaptoethanol) and human serum albumin. Reactions followed reversible biphasic kinetics, consistent with the presence of two electrophilic centers in NO_2-CLA located on the β- and δ-carbons with respect to the nitro group. The differential reactivity was confirmed by computational modeling of the electronic structure. The rates (k_{on} and k_{off}) and equilibrium constants for both reactions were determined for different thiols. LC-UV-Visible and LC-MS analyses showed that the fast reaction corresponds to β-adduct formation (the kinetic product), while the slow reaction corresponds to the formation of the δ-adduct (the thermodynamic product). The pH dependence of the rate constants, the correlation between intrinsic reactivity and thiol pK_a, and the absence of deuterium solvent kinetic isotope effects suggested stepwise mechanisms with thiolate attack on NO_2-CLA as rate-controlling step. Computational modeling supported the mechanism and revealed additional features of the transition states, anionic intermediates, and final neutral products. Importantly, the detection of cysteine-δ-adducts in human urine provided evidence for the biological relevance of this reaction. Finally, human serum albumin was found to bind NO_2-CLA both non-covalently and to form covalent adducts at Cys-34, suggesting potential modes for systemic distribution. These results provide new insights into the chemical basis of NO_2-CLA signaling actions.

Nitroalkene fatty acids are endogenous adaptive signaling mediators formed *in vivo* upon addition of nitric oxide ($NO^•$)- or nitrite (NO_2^-)-derived nitrogen dioxide ($NO_2^•$) to unsaturated fatty acids (1–3). The presence of the electron-withdrawing nitro group renders the nitroalkene β-carbon electron-deficient and thus susceptible to attack by nucleophiles in reversible Michael addition reactions (4). The electrophilicity of nitroalkene fatty acids is critical to the biological actions of these molecules, as demonstrated by the inhibitory effects of increased nitroalkene reductase activity (5). Nitroalkene fatty acids exhibit potent anti-inflammatory and cyto-protective properties and thus are beneficial in many models of disease, including atherosclerosis, restenosis, ischemia reperfusion, renal injury, diabetes, metabolic syndrome, and endotoxemia (6–13). Furthermore, endogenous formation of nitroalkene fatty acids has been associated with the cardioprotective effects of the Mediterranean diet (14, 15). Notably, the potential application of soft electrophiles as pharmacological agents is underscored by the Food and Drug Administration approval of dimethyl fumarate for the treatment of multiple sclerosis (16, 17).

Thiols are excellent nucleophiles and are able to react with different electrophiles, including oxidants. This property constitutes the basis of the fundamental roles of particular thiols in signaling, detoxification, and antioxidant response processes. For most chemical and enzymatic reactions, thiol reactivity involves the nucleophilic attack of the thiolate (RS^-) on the electrophile. The intracellular compartment presents an elevated concentration of reduced thiols. Glutathione (GSH) is the main low molecular weight thiol in the cytosol (2–17 mM), and protein thiols represent ~70% of the total reduced intracellular pool (18–21). In contrast, plasma has much lower total thiol concentrations that, in addition, are predominantly oxidized.

* This work was supported by grants and fellowships from Comisión Sectorial de Investigación Científica (Universidad de la República, Uruguay) (to L. T., M. N. M., and B. A.), Agencia Nacional de Investigación e Innovación (ANII, Uruguay) (to L. L.), National Institutes of Health Grants K01-HL133331 (to D. A. V.) and R01-AT006822 (to F. J. S.), and American Heart Association Grant in Aid 14GRNT20170024 (to F. J. S.). D. A. V., S. R. W., and F. J. S. acknowledge financial interest in Complexa Inc. The content is solely the responsibility of the authors and does not necessarily represent the official views of the National Institutes of Health.
◆ This article was selected as one of our Editors' Picks.
[S] This article contains supplemental Figs. S1 and S2 and Table S1.
[1] Both authors contributed equally to this work.
[2] Active members of the National System of Researchers and of PEDECIBA (Uruguay).
[3] To whom correspondence may be addressed: Laboratorio de Enzimología, Facultad de Ciencias. Iguá 4225, Montevideo 11400, Uruguay. Tel.: 598-2-525-0749; E-mail: beatriz.alvarez@fcien.edu.uy.
[4] To whom correspondence may be addressed: Dept. of Pharmacology and Chemical Biology, Thomas E. Starzl Biomedical Science Tower E1340, 200 Lothrop St., University of Pittsburgh, Pittsburgh, PA 15213. Tel.: 412-648-0193; Fax: 412-648-2229; E-mail: fjs2@pitt.edu.

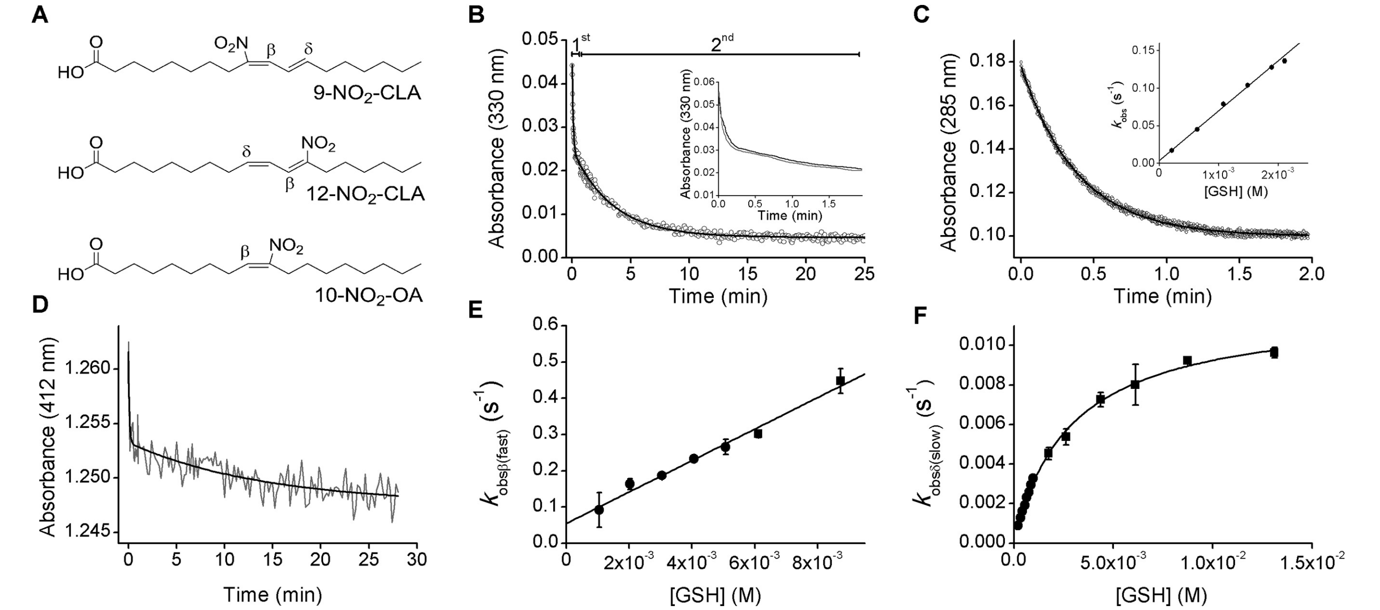

FIGURE 1. **Reactions of NO_2-CLA with thiols at pH 7.4.** *A*, structures of 9- and 12-NO_2-CLA and of 10-NO_2-OA showing the electrophilic β- or δ-carbons. *B*, a mixture of 9- and 12-NO_2-CLA (~10 μM) was mixed with GSH (3 mM) in phosphate buffer (0.1 M) containing DTPA (0.1 mM) at pH 7.4 and 25 °C, and the absorbance at 330 nm was registered. The *black trace* represents the best fit to a bi-exponential function. *Inset*, purified 9-NO_2-CLA (*black trace*) or 12-NO_2-CLA (*gray trace*) were mixed with GSH as in *B*. *C*, NO_2-OA (10 μM) was mixed with GSH (0.6 mM), and the absorbance at 285 nm was registered. *Inset*, k_{obs} values at increasing GSH concentrations (0.2–2 mM) were determined from the best fit to single exponential functions. The *symbols* represent the means ± S.E. ($n = 4$). Some *error bars* are smaller than the symbols. *D*, NO_2-CLA (~10 μM) was mixed with TNB (90 μM), and the absorbance at 412 nm was recorded. *E*, k_{obs} values for the fast phase of the reaction between NO_2-CLA and GSH were determined from kinetic traces as in *B*. Different *symbols* represent the means ± S.E. of representative independent experiments; *squares*, $n = 3$; *circles*, $n = 4$. *F*, same as in *E* but k_{obs} correspond to the slow phase; *circles*, $n = 1$; *squares*, means ± S.E., $n \geq 3$.

Low molecular weight plasma thiols include cysteine, cysteinylglycine, GSH, homocysteine, and γ-glutamylcysteine, which together constitute a total of 12–20 μM reduced thiol. The most abundant thiol in this compartment is cysteine 34 in human serum albumin (HSA)[5] which is ~600 μM and 75% reduced (22).

From a kinetic, mechanistic, and structure-reactivity relationship aspect, Michael addition and β-elimination reactions between various activated olefins and nucleophiles have received considerable attention in the literature. Depending on the nucleophilic and electrophilic partners as well as on the reaction conditions, two types of mechanisms have been proposed, concerted or stepwise, with the latter involving intermediate carbanions (23–26).

Conjugated linoleic acid (CLA) is a preferential substrate for biological nitration leading to the formation of 9- and 12-nitro-octadecadienoic acid (9- and 12-NO_2-CLA) (27). Nitroalkene derivatives of CLA are present in plasma and urine of healthy individuals with and without CLA supplementation and are generated during digestion, metabolic stress, and inflammation (1, 2, 27). The reaction between thiols and NO_2-CLA has implications for the modulation of not only signaling actions but also circulating levels and bio-elimination pathways (2, 6, 28). Importantly, in the case of NO_2-CLA, both the β- and δ-carbons with respect to the nitro group are, in principle, electrophilic and thus susceptible to reaction with nucleophiles.

Herein, we provide an experimental and computational study of the reaction of NO_2-CLA, the most abundant endogenous nitroalkene, with biological thiols. We found that two reversible products are formed, the β-adducts and the δ-adducts. The β-adducts are formed with faster kinetics, but the δ-adducts are more stable. The reaction mechanisms are stepwise, with thiolate attack on the nitroalkene being the rate-controlling step. In addition, HSA is able to bind NO_2-CLA non-covalently. Our findings contribute to the understanding of the chemical basis of the signaling and pharmacological actions of nitroalkene fatty acids.

Results

NO_2-CLA Reacts Biphasically and Reversibly with Low Molecular Weight Thiols—Stopped-flow mixing of a solution consisting of 9- and 12-NO_2-CLA (Fig. 1*A*) with excess GSH led to a reduction in absorbance at 330 nm, consistent with loss of double bond conjugation. The decrease was biexponential and included a fast phase that lasted ~0.5 min followed by a second phase that was slower by a factor of ~30 (Fig. 1*B*). No significant changes in absorbance occurred in the absence of thiols. Although the NO_2-CLA stock contains an ~1:1 mixture of the positional isomers 9- and 12-NO_2-CLA, the existence of two phases could not be explained by a differential reactivity of the isomers, as purified 9- and 12-NO_2-CLA yielded comparable biphasic kinetics (Fig. 1*B*, *inset*). In contrast, the reaction with the monounsaturated derivative nitro-oleic acid (NO_2-OA),

[5] The abbreviations used are: HSA, human serum albumin; CLA, conjugated linoleic acid; BME, β-mercaptoethanol; NO_2-CLA, nitro-conjugated linoleic acid; NO_2-OA, nitro-oleic acid; DTNB, 5,5′-dithiobis(2-nitrobenzoate); TNB, 5-thio 2-nitrobenzoate; DTDP, 4,4′-dithiodipyridine; DTPA, diethylenetriaminepentaacetic acid; NEM, *N*-ethylmaleimide; MRM, multiple reaction monitoring; TS, transition state; au, atomic unit; WBI, Wiberg bond index; NPA, natural population analysis; PA, proton affinity; MEP, molecular electrostatic potential; RC, reactants complex.

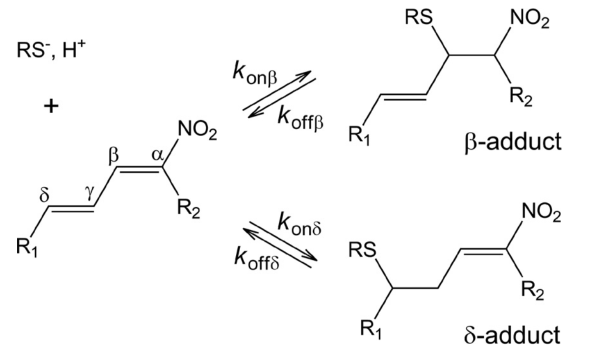

SCHEME 1. **Reactions between NO_2-CLA and low molecular weight thiols.** R_1 = $(CH_2)_5CH_3$ for 9-NO_2-CLA or $(CH_2)_7CO_2H$ for 12-NO_2-CLA; R_2 = $(CH_2)_7CO_2H$ for 9-NO_2-CLA or $(CH_2)_5CH_3$ for 12-NO_2-CLA, RS^- = thiolate.

which has only one electrophilic site, was monophasic (Fig. 1*C*) (29). When NO_2-CLA was mixed with the yellow thiol thionitrobenzoate (TNB), which allows us to follow changes in thiol concentration due to its absorbance at 412 nm, the kinetics were also biphasic, confirming that thiol consumption occurred in both phases (Fig. 1*D*). Regarding the concentration dependence of the reaction between NO_2-CLA and excess GSH, a linear dependence with a non-zero *y* axis intercept was observed between the pseudo-first order rate constant (k_{obs}) of the fast phase and GSH concentration (Fig. 1*E*), while a hyperbolic dependence with a non-zero intercept was observed for the slow phase (Fig. 1*F*).

Taken together, the kinetic results are consistent with two parallel and reversible processes involving two non-equivalent electrophilic centers in NO_2-CLA. These centers react with thiols forming two products that we hypothesize are the β- and the δ-adducts as shown in to Scheme 1, where $k_{on\beta}$ and $k_{on\delta}$ are second-order rate constants at pH 7.4 for the forward addition reaction of the fast and slow processes, respectively, and $k_{off\beta}$ and $k_{off\delta}$ correspond to first-order rate constants for the reverse elimination reactions.[6]

The coupled differential equations derived from Scheme 1 can be solved in matrix form yielding complex biexponential concentration functions. The relation of the exponential constants k_{obs} with the rate constants and concentrations is simplified when one phase is faster than the other (30, 31). In this case, the larger exponential constant, $k_{obs(fast)}$, increases linearly with thiol concentration according to Equation 1 (Fig. 1*E*).

$$k_{obs(fast)} = k_{on\beta}[\text{thiol}] + k_{off\beta} \qquad \text{(Eq. 1)}$$

For GSH reactions, $k_{on\beta} = 34 \pm 4\ \text{M}^{-1}\ \text{s}^{-1}$ was determined from the slope of the plot, whereas $k_{off\beta} = 0.10 \pm 0.02\ \text{s}^{-1}$ was obtained from the *y* axis intercept. The equilibrium dissociation constant ($K_{eq\beta}$) was calculated by dividing $k_{off\beta}$ by $k_{on\beta}$ and its value was $(2.8 \pm 0.9) \times 10^{-3}$ M (25 °C, pH 7.4).

The smaller exponential constant, $k_{obs(slow)}$, is given by the sum of the forward and reverse effective rate constants, where the former is $k_{on\delta}$ [thiol] multiplied by the fraction of free NO_2-CLA, and it increases hyperbolically with thiol concentration according to Equation 2 (Fig. 1*F*).

[6] $k_{on\beta}$ and $k_{on\delta}$ are $k_{on\beta,\ pH\ 7.4}$ and $k_{on\delta,\ pH\ 7.4}$, the apparent rate constants at pH 7.4. The same applies to $k_{off\beta}$ and $k_{off\delta}$. The notation was simplified for clarity.

$$k_{obs(slow)} = \frac{k_{on\delta}K_{eq\beta}[\text{thiol}]}{K_{eq\beta} + [\text{thiol}]} + k_{off\delta} \qquad \text{(Eq. 2)}$$

From fits to this equation, the $k_{on\delta}$ for the reaction with GSH was determined to be $3.5 \pm 0.5\ \text{M}^{-1}\ \text{s}^{-1}$ whereas $K_{eq\beta}$ was $(3.0 \pm 0.2) \times 10^{-3}$ M, in excellent agreement with the value determined from the fast phase. The $k_{off\delta}$ was obtained using data at relatively low thiol concentrations and was $(3 \pm 1) \times 10^{-4}\ \text{s}^{-1}$. The $K_{eq\delta}$ was $(9 \pm 4) \times 10^{-5}$ M.

Similar determinations were carried out for cysteine, homocysteine, cysteinylglycine, and β-mercaptoethanol (BME), and the rate and equilibrium constants are shown in Table 1. The rate constants were higher for the presumed β-adducts in all cases. The equilibrium constants were lower by factors of 20–65 for the δ-adducts, reflecting higher stability. It is worth mentioning that at higher cysteine concentrations (30 mM) a third slow phase became evident ($k_{obs} = (1.33 \pm 0.01) \times 10^{-3}\ \text{s}^{-1}$), which was not further characterized. No reaction was observed with histidine ($\leq$40 mM), suggesting that additions of α-amino and imidazole groups were not significant, consistent with nitrogenous bases being weaker nucleophiles toward Michael acceptors than thiolates (23, 26).

NO_2-CLA Has Two Non-equivalent Electrophilic Carbon Centers in C_β and C_δ—The electrophilic Fukui $f^+(r)$ function, which measures the propensity of NO_2-CLA to gain electron density in a nucleophilic attack, is shown in Fig. 2, mapped on a total electronic density isosurface calculated at the PCM-DFT level in aqueous solution. Two well defined and distinct soft electrophilic regions (Fig. 2, depicted in *blue*) involving the C_β and C_δ centers are found in both isomers. Whereas the region around C_β appears extended over the molecular surface and connected to the electrophilic nitro group envelope, the region enclosing C_δ is considerably smaller. These features would make C_β more prone to nucleophilic attack by thiols. Atomic softness data calculated from global softness and condensed Fukui f_A^+ (Table 2) completes the picture enabling a quantitative comparison, showing that C_β is significantly softer than C_δ, establishing the non-equivalency of the electrophilic C_β and C_δ centers and contributing to consolidate the hypothesis of their association with the fast and slow reactions, respectively.

The β-Adduct Is the Kinetic Product and the δ-Adduct Is the Thermodynamic Product—To define the products generated in each phase of the reaction, spectrophotometric, LC-UV-Visible, and LC-MS/MS experiments were performed. First, the time course of the reaction with GSH was followed at three different wavelengths. During the fast phase, the decrease in absorbance at 330 nm correlated with an increase at 250 nm, although no changes were observed at 290 nm. In the slow phase, however, the decrease at 330 nm correlated with an increase at 290 nm (Fig. 3*A*). These results suggest that the product formed during the slow reaction contains an intact nitroalkene moiety due to thiol addition at the δ-carbon (29, 32) whereas that formed during the fast reaction does not.

LC-UV-Visible analyses were performed using BME as a model thiol due to its slower addition kinetics and better chromatographic separation (33, 34). 9-NO_2-CLA eluted at a retention time of 15.5 min (peak 1, λ_{max} 320 nm) (Fig. 3, *B* and *C*).

TABLE 1

Apparent rate and equilibrium constants at pH 7.4 (25 °C) of the reaction of NO_2-CLA with thiols

Thiol[a]	Fast reaction (β)			Slow reaction (δ)			pK_a[b]
	$k_{on\beta}$	$k_{off\beta}$	$K_{eq\beta}$	$k_{on\delta}$	$k_{off\delta}$	$K_{eq\delta}$	
	$M^{-1}s^{-1}$	s^{-1}	$M (\times 10^{-3})$	$M^{-1}s^{-1}$	$s^{-1} (\times 10^{-4})$	$M (\times 10^{-4})$	
Glutathione	34 ± 4[c]	0.10 ± 0.02[c]	2.8 ± 0.9	3.5 ± 0.5[d]	3 ± 1[e]	0.9 ± 0.4	8.94
Glutathione (9-NO_2-CLA)	33 ± 7[f]	0.12 ± 0.02[f]	4 ± 1	3.5 ± 0.3[f]	ND[g]	ND[g]	
Glutathione (12-NO_2-CLA)	31 ± 8[f]	0.15 ± 0.02[f]	5 ± 2	5.6 ± 0.6[f]	ND[g]	ND[g]	
Glutathione (NO_2-OA)	64 ± 1[f]	$(6 \pm 1) \times 10^{-3}$[f]	0.09 ± 0.02	Absent	Absent		
Cysteine	32.6 ± 0.2[h]	0.196 ± 0.002[h]	6.0 ± 0.1	2.8 ± 0.4[e]	6 ± 3[e]	2 ± 1	8.29
Homocysteine	18.9 ± 0.5[e]	0.03 ± 0.02[e]	2 ± 1	1.4 ± 0.2[e]	1 ± 1[e]	1 ± 1	9.10
Cysteinylglycine	51 ± 4[h]	0.28 ± 0.06[h]	5 ± 2	10 ± 2[e]	10 ± 5[f]	1.0 ± 0.7	7.95
β-Mercaptoethanol	15 ± 2[h]	0.019 ± 0.005[h]	1.3 ± 0.6	3.0 ± 0.4[e]	0.6 ± 0.5[e]	0.2 ± 0.2	9.60
Thionitrobenzoate[i]	~800	ND[g]		~50	ND[g]		

[a] A mixture of 9- and 12-NO_2-CLA was used unless otherwise specified.
[b] Thiol pK_a values reported in Ref. 36.
[c] Values are the means± S.E. of $n = 4$ independent experiments.
[d] Values are the means± S.E. of $n = 5$ independent experiments.
[e] Values are the means± S.E. of $n = 3$ independent experiments.
[f] $n = 1$, values are the parameter ± error of the fit.
[g] ND is not determined.
[h] Values are the means ± S.E. of $n = 2$ independent experiments.
[i] Because of the high absorptivity of TNB, only rough estimates of k_{on} could be obtained.

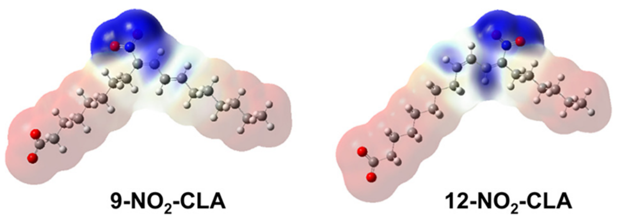

FIGURE 2. **Electrophilic centers in 9-/12-NO_2-CLA regioisomers.** Fukui $f^+(r)$ function for nucleophilic attack mapped on a total electron density surface of 0.0004 au as determined in aqueous solution at the PCM(IEF)-ωB97X-D/6-31+G(d,p) level of theory. Positive areas depicted in *blue* represent the electrophilic regions. The coloring scheme spans from -6.0×10^{-7} au in *red* to 1.1×10^{-4} au in *blue*.

TABLE 2

Atomic softness s_A^+ for the carbon centers in the conjugated nitroalkene moieties embedded in each NO_2-CLA regioisomer (in au)

Data were determined according to Equation 10. Positive values correspond to atoms more prone to receive electrons, acting as electrophilic centers. The softest and most reactive C_β site in each isomer is underlined.

Regioisomer	Carbon center			
	C_α	C_β	C_γ	C_δ
9-NO_2-CLA	−0.036	<u>0.684</u>	−0.113	0.462
12-NO_2-CLA	−0.029	<u>0.699</u>	0.117	0.523

The peak at 15.1 min (peak 1*) corresponds to contaminant 12-NO_2-CLA (data not shown). In the first 10 s of the reaction with BME, a peak appeared at 8.8 min (peak 2, λ_{max} 240 nm) (Fig. 3, *B*, *inset,* and *C*) that was still present after 5 min but disappeared after 1 h due to the reverse elimination process and further reactions of NO_2-CLA, and it was thus assigned to the fast reaction product (β-addition). After 5 min of reaction, another peak appeared at 8.2 min (peak 3, λ_{max} 280 nm) (Fig. 3*B*), became dominant as the reaction progressed, and was assigned to the δ-addition product. This peak was not symmetric, suggesting the presence of two diastereomers, both with maximum absorbances at 280 nm (Fig. 3*C*). The secondary peaks at 8.6 (peak 2*) and 7.7 min (peak 3*) were assigned to the products of the fast and slow processes for the reaction between contaminant 12-NO_2-CLA and BME.

To obtain further mechanistic insight, the reaction between purified 9-NO_2-CLA and BME was monitored by LC-MS/MS. Fig. 4, *A* and *B,* shows that 9-NO_2-CLA consumption (MRM 324/46, retention time: 8.6 min) leads to the formation of an early addition product (MRM 402/324, retention time: 6.9 min, β-adduct), which decays and becomes undetectable at 60 min. The disappearance of this product coincides with the formation of two isobaric species (MRM 402/324, retention times: 6.5 and 6.8 min, δ_1- and δ_2-adducts, respectively) that become the dominant products during the slow phase of the reaction and likely represent diastereomers as further discussed below (Figs. 6*C* and 7*B*). To confirm the relative rates of elimination from the adducts formed during the different phases of the reaction, aliquots were incubated with excess NEM (100 mM, 30 min) to efficiently trap BME ($k = 7 \times 10^4$ $M^{-1}s^{-1}$ at pH 7.4 (35)) (Fig. 4, *C* and *D*). Consistent with the measured $k_{off\beta}$ and $k_{off\delta}$ values (Table 1), NEM incubation completely reversed adducts formed at early time points but had no effect on the late products. Similar results were obtained with the purified 12-NO_2-CLA isomer, with the particularity that only one δ-addition product could be resolved to such an extent as to allow reliable peak integration (supplemental Fig. S1).

Overall, LC-MS/MS results and UV-Visible analysis were in excellent agreement, and it was concluded that the fast reaction corresponded to the β-addition of the thiol and the slow reaction to the δ-addition (Scheme 1). No evidence for the formation of other products was obtained. The results are consistent with a fast reaction of NO_2-CLA with the thiol to form initially the β-adduct. Because of the reversibility of this reaction, the β-adduct undergoes elimination and releases free NO_2-CLA, which engages in further reactions finally leading to the slow accumulation of the more stable δ-adduct.

Addition Requires a Thiolate and Elimination Occurs through Two Independent Pathways—The pH dependence of the reaction kinetics of NO_2-CLA with GSH was studied using three-component buffers of constant ionic strength. Plots of k_{obs} *versus* GSH concentration were constructed at each pH, from which the corresponding apparent $k_{on,\,app}$ and $k_{off,\,app}$ values were obtained for both fast and slow processes. For the fast reaction, the $k_{on\beta,\,app}$ increased with pH (Fig. 5*A*) according to a single pK_a equation (Equation 3),

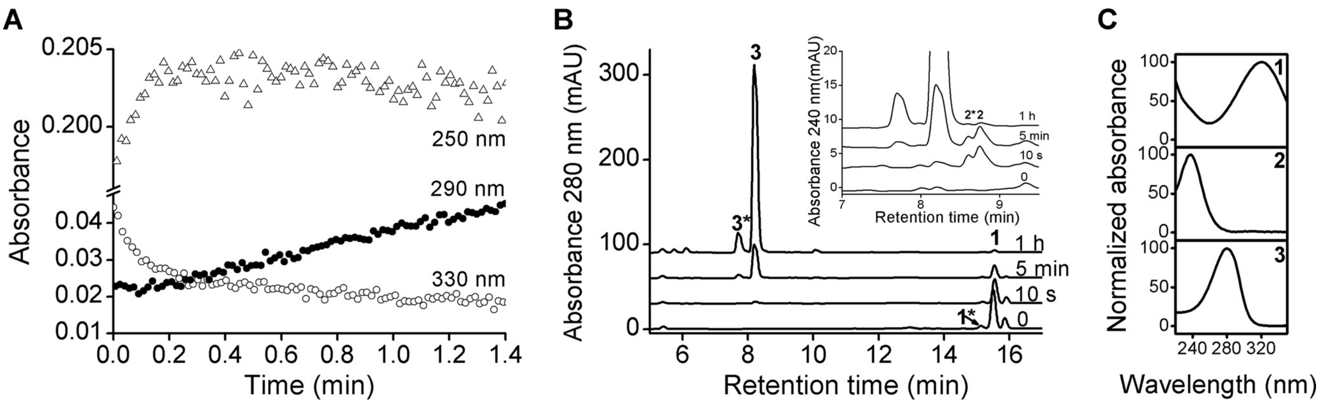

FIGURE 3. **UV-Visible analysis of the reaction between NO_2-CLA and thiols.** *A*, time course changes in absorbance at 330 (*open circles*), 290 (*black circles*), and 250 nm (*open triangles*) for the reaction between NO_2-CLA (10 μM) and GSH (3 mM). *B*, representative LC-UV-visible traces of the reaction between purified 9-NO_2-CLA (100 μM) and BME (1.76 mM). Aliquots were obtained at the indicated time points before LC-UV-visible analysis. *C*, UV-visible spectra for 9-NO_2-CLA (*panel 1*) and both β- (*panel 2*) and δ-adducts (*panel 3*). *Asterisks* indicate minor peaks derived from contaminant 12-NO_2-CLA.

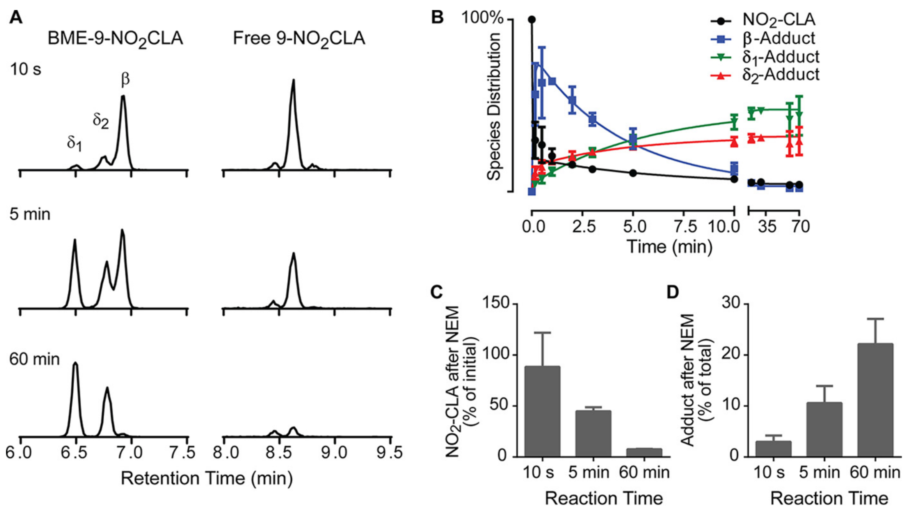

FIGURE 4. **LC-MS/MS analysis of the reaction between NO_2-CLA and BME.** *A*, purified 9-NO_2-CLA (10 μM) was reacted with BME (1.76 mM), and aliquots were obtained at 10 s (*top*), 5 min (*middle*), and 60 min (*bottom*) for analysis of free NO_2-CLA (*right*) and BME-NO_2-CLA adducts (*left*). *B*, representative time course for 9-NO_2-CLA reaction with BME. *C* and *D*, aliquots collected at the indicated times were incubated with NEM (100 mM), and the percentage of free NO_2-CLA with respect to that at time 0 (*C*) and the percentage of BME-NO_2-CLA adduct with respect to NEM-untreated controls (*D*) were determined. Data are representative of three independent experiments.

$$k_{\text{on, app}} = k_{\text{on, pH-indep}} \frac{K_a}{K_a + [\text{H}^+]} \quad \text{(Eq. 3)}$$

where $k_{\text{on, pH-indep}}$ represents the rate constant for the completely ionized thiol. The pK_a was 8.78 ± 0.02, in agreement with the reported pK_a of GSH (8.94 (36)) and consistent with the requirement for rapid prior ionization of the thiol to thiolate in the forward addition process. The $k_{\text{off}\beta,\text{ app}}$ presented an upward bend indicating that the elimination process occurs through two independent pathways (Fig. 5*B*) (37). At biologically relevant pH values, elimination appears to be unimolecular or water-assisted. The increase above pH 9 likely reflects the assistance of alternative bases. Similar pH dependences were observed for the slow phase (data not shown), suggesting that comparable mechanisms are operative.

Correlations with Thiol pKa Suggest That the Thiolate Participates in the Rate-controlling Step—Because the thiolate is the reactant in the forward addition process, the $k_{\text{on, app}}$ values at pH 7.4 (Table 1) were corrected according to Equation 3 to obtain pH-independent values ($k_{\text{on, pH-indep}}$), that reflect the intrinsic reactivity of each thiolate toward NO_2-CLA. For the fast reaction, the log of $k_{\text{on, pH-indep}}$ increased with thiol pK_a according to Equation 4,

$$\log k_{\text{on, pH-indep}} = \beta_{\text{nuc}} \text{p}K_a + C_{\text{on}} \quad \text{(Eq. 4)}$$

where β_{nuc} is the Brønsted nucleophilic coefficient, and C_{on} is a constant. According to the slope and the *y* axis intercept of the plot, β_{nuc} was 0.64 ± 0.08, and C_{on} was −2.8 ± 0.7 (Fig. 5*C*, *top trace*).The β_{nuc} value of 0.64 indicates that thiolate nucleophilicity correlates with proton basicity and is consistent with thiolate participation in transition state formation. It also suggests a relatively high degree of charge transfer at the transition state level. For comparison, β_{nuc} values of 0.45 and 0.16 were reported for the addition of thiols to acrylonitrile (26) and α-nitrostilbene, respectively (23).

For the reverse reaction (pH $<$9), inverse correlations between the log k_{off} and thiol pK_a were obtained, consistent with Equation 5,

$$\log k_{\text{off}} = \beta_{\text{lg}} \text{p}K_a + C_{\text{off}} \quad \text{(Eq. 5)}$$

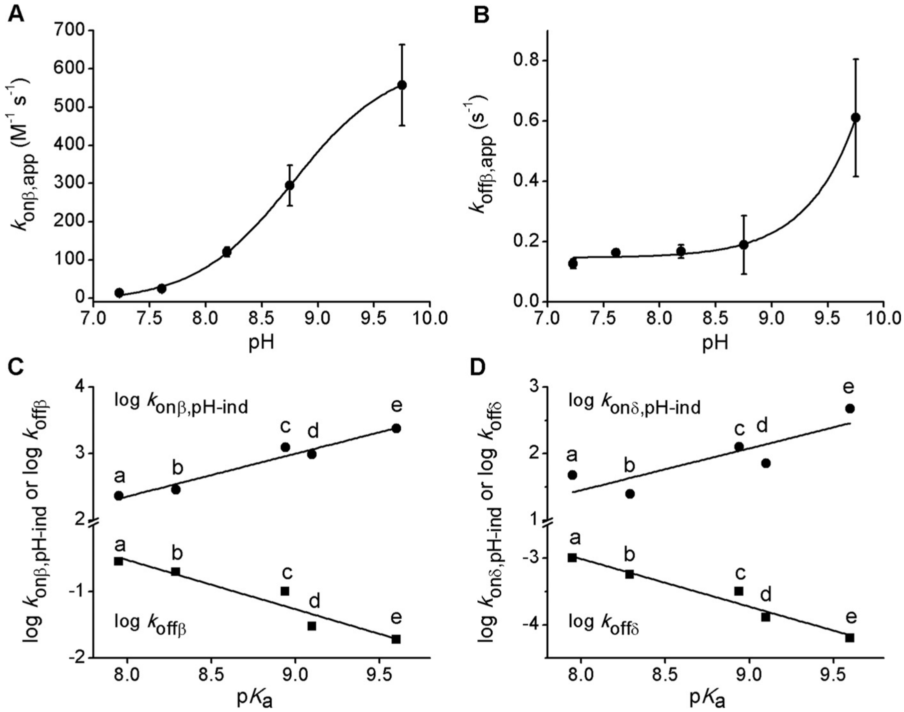

FIGURE 5. **pH-dependence and correlations with thiol pK_a.** *A* and *B,* fast reaction between GSH and NO_2-CLA was studied at different pH values using three-component constant ionic strength buffers. Apparent $k_{on\beta}$ (*A*) and $k_{off\beta}$ (*B*) values were obtained as in Fig. 1*E* and Equation 1 from the fit of plots of k_{obs} *versus* GSH concentration to a straight line; the *error bars* represent the standard error of the fit. *C* and *D,* Brønsted plots for fast (*C*) and slow (*D*) reactions. The logarithm of $k_{on,\ pH\text{-}indep}$ rate constants (*circles,* calculated from k_{on} values at pH 7.4) and k_{off} (*squares*) were plotted against thiol pK_a values. Data are from Table 1; *a,* cysteinylglycine; *b,* cysteine; *c,* GSH; *d,* homocysteine; *e,* BME.

where β_{lg} is the Brønsted leaving group coefficient, and C_{off} is a constant. The values of β_{lg} and C_{off} were determined from the slope and *y* axis intercept of the plot to be -0.73 ± 0.12 and 5.3 ± 1.1, respectively (Fig. 5*C, bottom trace*). The β_{lg} value of -0.73 indicates that the reactivity of the adduct correlates with the proton acidity of the thiol that is eliminated. This is consistent with a rate-controlling step that involves thiolate departure and partial charge formation, with considerable amount of C–S bond breaking in the transition state, in agreement with a reversal of the mechanism proposed for the forward reaction. Values of β_{lg} of -0.68 and -0.54 were reported for the elimination of thiols from α-nitrostilbene and acrylonitrile adducts, respectively, with leaving group expulsion argued to be the rate-controlling step in the latter case (23, 25). For the slow reaction, similar trends were observed, with $\beta_{nuc} = 0.6 \pm 0.2$, $C_{on} = -4 \pm 2$, $\beta_{lg} = -0.72 \pm 0.09$, and $C_{off} = 2.7 \pm 0.8$ (Fig. 5*D*).

Lack of Solvent Kinetic Isotope Effects—The reaction of 20 μM NO_2-CLA with 4 mM GSH exhibited k_{obs} of 0.23 ± 0.03 and $(6.4 \pm 0.2) \times 10^{-3}\ s^{-1}$ for the fast and slow processes, respectively. When H_2O was replaced by D_2O (92%) and the pD was adjusted for similar GSH ionization fractions, k_{obs} values were 0.25 ± 0.04 and $(6.1 \pm 0.3) \times 10^{-3}\ s^{-1}$, indicating the absence of significant deuterium solvent kinetic isotope effects. This rules out rate-controlling steps that involve protonation and suggests that concerted addition-elimination processes are not involved. Instead, the reactions likely occur through stepwise mechanisms involving anionic intermediates and thiolate attack as the rate-limiting step, in agreement with the Brønsted correlations shown in Fig. 5, *C* and *D*.

Main Features of the Transition States and Anionic Intermediates for Thiolate Addition on C_β/C_δ Centers—In line with the experimental results, PCM-DFT modeling provided a detailed characterization of the transition states (TS_β/TS_δ) and anionic intermediates (I_β/I_δ) for a stepwise attack by a thiolate on C_β/C_δ electrophilic centers embedded at the common central moiety of both NO_2-CLA isomers (Fig. 6 and structural data in supplemental Table S1). No evidence was found here for a concerted four-membered ring TS as reported for the attack of thiols on α,β-unsaturated carbonyls (38). Both TS_β/TS_δ resemble the open structures found for thio-Michael addition on that kind of acceptor (39, 40), taking place after fast deprotonation of the thiolate in solution.

Reactions at C_β and C_δ proceed both through entropically disfavored loose reactant complexes (RC_β/RC_δ, Fig. 6, *A* and *B*) leading to transition states (TS_β/TS_δ) with a more asymmetric distribution of charge in the acceptor and associated free-energy barriers of 18.9 and 20.2 kcal/mol, respectively, calculated with respect to the isolated reactants in solution (Table 3). This supports the assignment of β-/δ-addition processes, respectively, to the fast/slow phases observed in the experiments. In fact, a difference of 1.3 kcal/mol in activation free-energy translates into a 9-fold increase in the k_{on} rate for β-addition with respect to δ-addition, in excellent agreement with the kinetic experiments (Table 1). Charge transfer of 0.33 and 0.28 atomic units (au) between reacting moieties is respectively found at TS_β and TS_δ (mainly accommodated at the NO_2 group) reflecting the similarity between β_{nuc} parameters for both fast and slow NO_2-CLA reactions. The *R*1/*R*2 substituents at the conju-

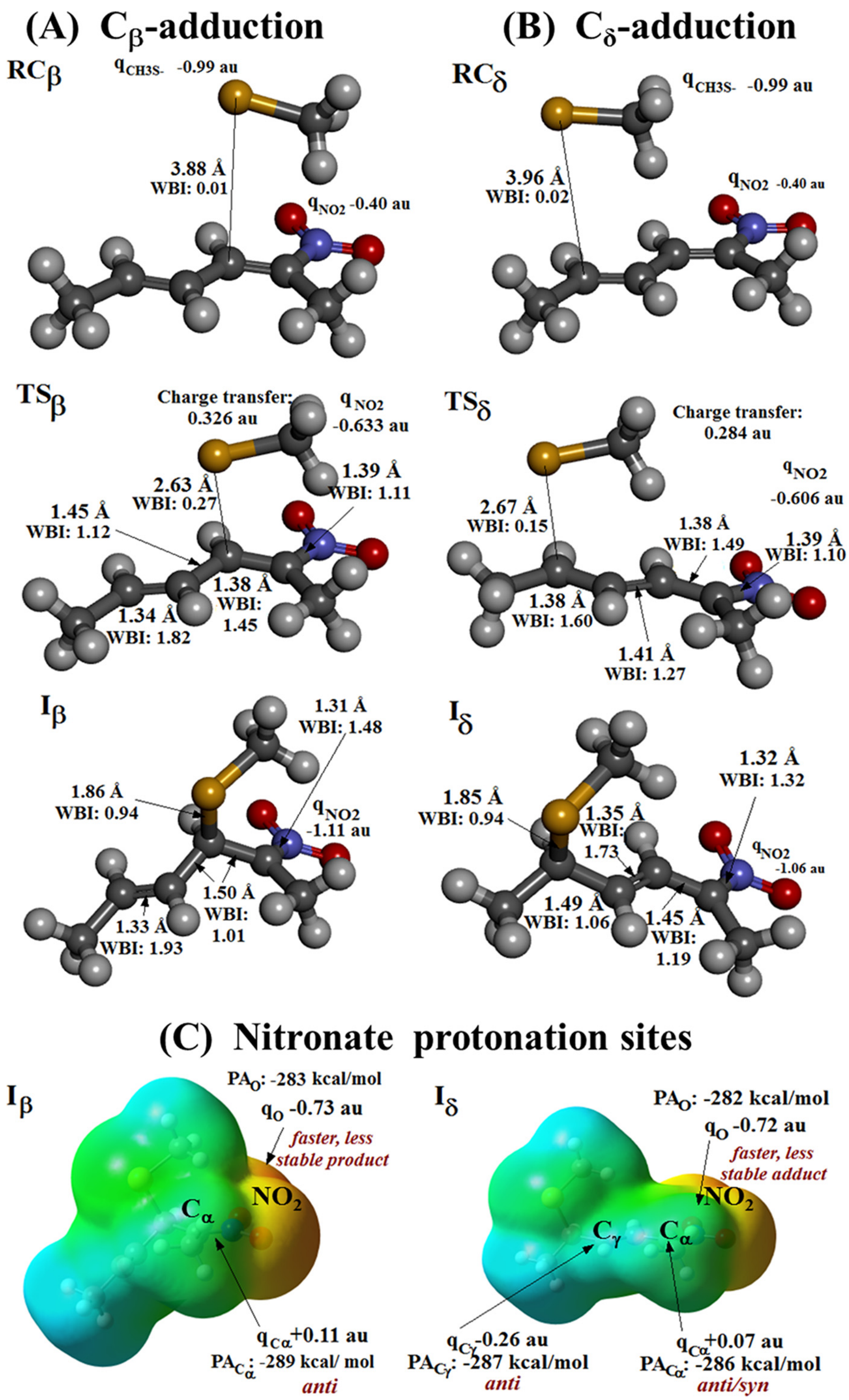

FIGURE 6. **Structural features of the species involved in β- and δ-adduction as determined by PCM-DFT modeling in aqueous solution using CH_3S^- as representative thiol and a model 2-nitrohexa-2,4-diene compound containing the reactive region of NO_2-CLA.** *A* and *B*, reactants complex, transition state, and nitronate intermediate, respectively, characterized for thiolate β-adduction (RC_β, TS_β, and I_β) or δ-adduction (RC_δ, TS_δ, and I_δ). Atoms are colored by element, and a selection of relevant bond lengths, WBI, and NPA atomic/group charges labeled as q_X (*X* represents an atom or group of atoms) featuring geometrical and electronic reorganization along each reaction channel is highlighted in proximity to the structures. Net charge transfer between reactants is evidenced at each TS. *C*, relevant properties toward I_β/I_δ nitronate protonation: MEP mapped on a total electron density surface of 0.004 au (notice that the underlying structures retain the orientation shown immediately above in *A* and *B* for each species), NPA atomic charges, and proton affinities (*PA*) at each O/C protonation site. All properties calculated at the PCM(IEF)-ωB97X-D/6−31+G(d,p) level in aqueous solution. MEP coloring scheme spans from −0.245 (*red*) to −0.04 au (*cyan-blue*). Although electrostatics favor a faster protonation at NO_2 oxygens in both cases, $C_{\alpha/\gamma}$ targets lead to more stable products, displaying mostly anti stereochemistry due to steric restrictions, as evidenced in *red labels*.

TABLE 3

Relative energetics of the species participant in β/δ-channels using a representative conjugated nitroalkene model

Enthalpy and Gibbs free-energy at 298 K and 1 atm relative to isolated reactants for each species involved in the stepwise mechanism for the thio-Michael addition and further protonation are calculated at the PCM(IEF, water)-ωB97X-D/6-31+G(d,p) level and expressed in kilocalories/mol. Free-energy reaction barrier for the first step and stability of the main Michael adduct(s) corresponding to each of the reaction channels are highlighted in boldface.

		Thiolate adduction step[a]				Protonation step, final products[b]		
Reaction Channel	Property	RC_X	TS_X	I_X		Aci-Nitro (O-protonated)	Nitroalkane (Cα-protonated)	Nitroalkene (Cγ-protonated)
β-Adduction	ΔH	2.6	6.5	−8.4	Kinetic product	−289.5	−297.3	Not formed
	ΔG	12.5	**18.9**	3.9		−278.7	**−284.9**	
δ-Adduction	ΔH	2.8	7.6	−14.5	Thermodynamic product	−294.8	−299.8	−300.4
	ΔG	11.6	**20.2**	**−1.5**		−283.1	**−287.7**	**−288.4**

[a] X = β or δ, see the corresponding structures in Fig. 6.
[b] See the corresponding structures in Fig. 7.

gated nitroalkene moiety (Scheme 1) modulate its intrinsic reactivity toward thiolate attack (23, 26). In particular, for nitroalkene fatty acids the alkyl/carboxyl(ate) chains are expected to increase the reactivity toward thio-Michael addition with respect to the model system studied here, without altering the mechanism[7] leading to a more pronounced charge reorganization between partners at the C_β/C_δ adduction TSs, closer to the expectations from the β_{nuc} values derived from experimental data. A similar rationale applies to bond forming/breaking at each TS, for which Wiberg bond indices (WBIs) of 0.27/0.15 for the nascent S···C_β/S···C_δ bonds imply advances of 28 or 16% at each reaction involving the model compounds. A lag in S–C_δ bond formation with respect to the advance in charge transfer from thiolate to nitroalkene moieties (not found in TS_β) may explain the higher barrier found for the slower reaction leading to the δ-adduct (41).

Concerning the anionic intermediates (I_β/I_δ, Fig. 6), they both would be nitronate species, sharing a strengthened C_α–N bond (WBIs: 1.48 and 1.32 au, respectively) and a net charge of −1 au localized at the NO_2 moiety in their structures. Whereas the second NO_2-CLA unsaturation remains intact at C_γ=C_δ in I_β, it appears shifted into C_γ=C_β, in I_δ enabling a more extended electron delocalization that translates in a more stable δ-intermediate (Table 3). No evidence of formation of any stable carbanion was found. The NO_2 group progressively captures all the electronic density transferred between reactants up to completion of each of these two parallel adduction processes, resulting in completely formed C–S single bonds (1.85–1.86 Å and WBIs 0.94 au) and loss of planarity at C_β/C_δ. Thus, whereas a thermodynamically disfavored nitronate I_β is obtained through a faster and slightly endoergic (but exothermic) process, the more stable I_δ would be the prevalent outcome of the adduction step in the longer timescales. Reverse free-energy reaction barriers in the range of 15–22 kcal/mol (Table 3) are indicative of reversible processes leading in both cases to elimination of a thiolate, more facilitated from the β-intermediate (once again a result qualitatively in line with the relationship between k_{off} values obtained for the fast/slow processes).

As a required step in reaching neutral products for these processes, protonation of the anionic intermediates has to be placed in the mechanistic scheme. Natural population analysis (NPA) atomic charges at C_α/C_γ/O, the corresponding proton affinities ($PA_{C\alpha}$, $PA_{C\gamma}$, and PA_O), and the molecular electrostatic potential (MEP) mapped on the molecular surface are shown in Fig. 6*C* as the properties of I_β/I_δ nitronates that determine the kinetics and thermodynamics of proton capture in aqueous solution. Two possibilities arise here (Fig. 7) as follows: O-protonation leading to an aci-Nitro R′CR=NO_2H derivative (aci-Nitro β-/δ-adducts) and $C_\alpha/_\gamma$-protonation leading to nitroalkane/nitroalkene products (tautomers of the former). A protonation preference for the O-site over the C_α-site has been shown for phenylnitromethanes both by experiments under acidic and neutral conditions in aqueous solution and methanol (42–44) and by computational modeling at the B3LYP/6-31+G(d,p) level in gas phase (42) or mimicking aqueous solution by including two water molecules in the system (45). The latter study also presented a water-assisted mechanism for conversion of aci-Nitro species toward a nitroalkane C_α tautomer, more stable by 8.3 kcal/mol (45). PCM(IEF)-ωB97X-D/6-31+G(d,p) modeling in the aqueous solution conducted here on the protonation of I_β and I_δ showed both species to be more prone for O-protonation (aci-Nitro would be thus a kinetic outcome of protonation), but all the C-protonated tautomers were found to be more stable by 5–6 kcal/mol than their aci-Nitro counterparts. Among the final species derived from I_δ, a small 0.7 kcal/mol difference in stability would favor a C_γ-protonated nitroalkene over a C_α-protonated and unsaturated nitroalkane, with the former being the most stable product achievable by all means.

Regarding stereoisomerism, while protonation at C_α must be anti-periplanar to the C_β–S bond linking the thiolate moiety that blocks any *syn* approach to I_β (only (*R,S*) or (*S,R*) enantiomers can be obtained among β-adducts), both *syn/anti* protonation appears feasible at the more accessible C_α position in I_δ (Fig. 6) yielding either (*R,R*), (*R,S*), (*S,R*), or (*S,S*) stereoisomers, an outcome that makes it possible to find enantiomers and diastereomers among the final δ-adducts.

Thus, on the basis of our calculations, a faster O-protonation of I_β/I_δ that would be followed by water-assisted tautomerization into the corresponding more stable counterparts complete the mechanism of reaction leading to the final products. According to modeling, the expected products would be then a β-thio-Michael-unsaturated adduct in nitroalkane form (Fig. 7*A*) in the short timescale and a mix of δ-thio-Michael adducts, including a prevalent nitroalkene form and two companion diastereomeric unsaturated nitroalkane species (Fig. 7*B*), in the long timescale.

[7] E. L. Coitiño, D. Pérez-Escanda, and F. Ferraro, unpublished data.

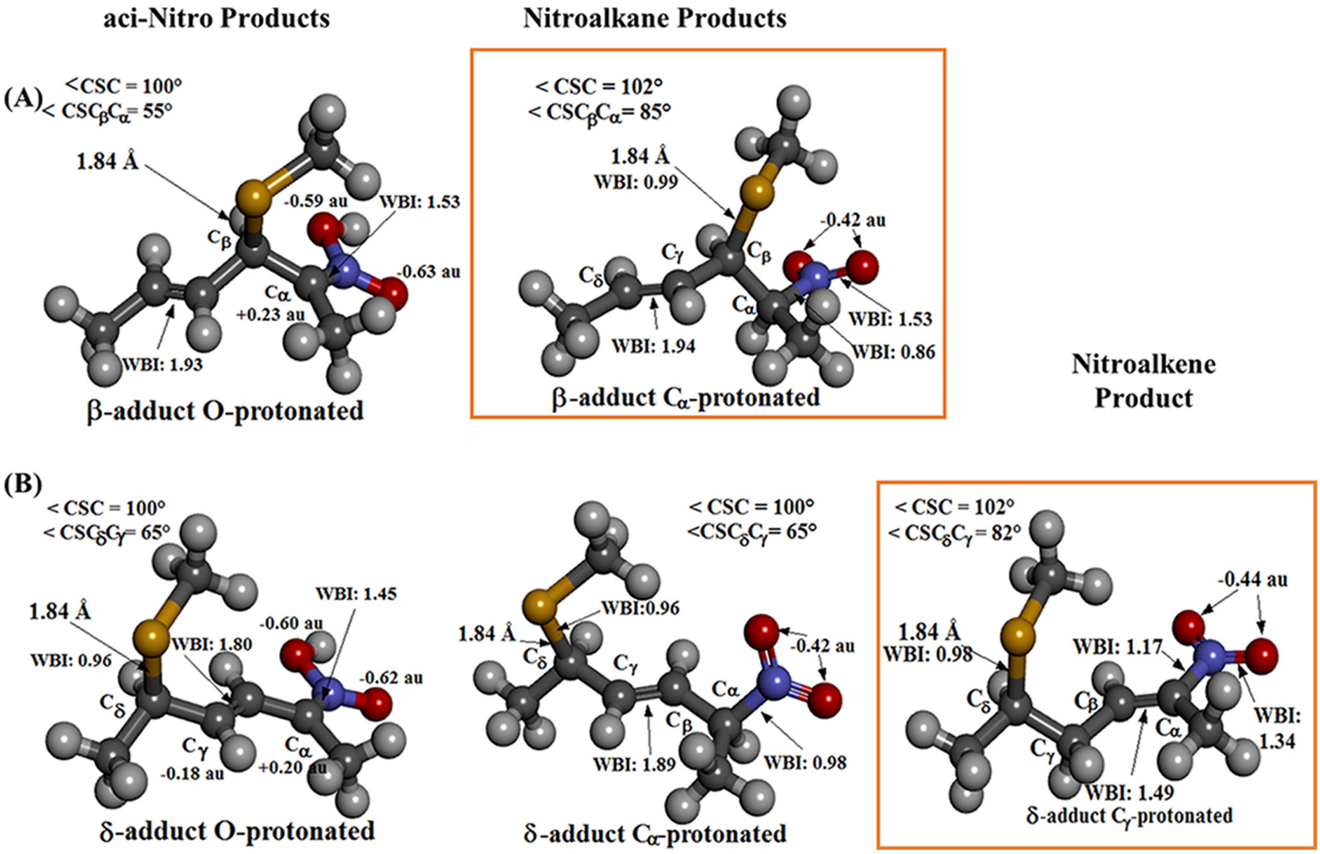

FIGURE 7. **Structural features of the possible neutral products characterized at the PCM(IEF)-ωB97X-D/6-31+G(d,p) level in aqueous solution.** *A*, O-protonated aci-Nitro and Cα-protonated nitroalkane β-adducts. *B*, O-protonated aci-Nitro, Cα-protonated nitroalkane, and Cγ-protonated nitroalkene δ-adducts. Atoms are colored by element, and a selection of the more relevant bond lengths and angles, WBIs, and NPA atomic charges on O, Cα, and Cγ obtained at the same level of theory are reported in the proximity of relevant bonds and atoms at each structure. The expected kinetic and thermodynamic prevalent products (Cα-protonated nitroalkane β-adduct and Cγ-protonated nitroalkene δ-adduct, respectively) are framed in *orange*.

NO_2-CLA-Cysteine δ-Addition Products Are Found in Human Urine—Based on experimental and modeling results, endogenous Cys-NO_2-CLA in human urine is expected to be primarily represented by the more stable δ-addition products. Isotopically labeled Cys-9-NO_2-CLA and Cys-12-NO_2-CLA enriched in δ-adducts were synthesized, mixed in a 1:1 ratio, and compared with urinary Cys-NO_2-CLA (Fig. 8). LC-MS/MS analysis is consistent with a predominant presence of the Cys-δ-adducts of 9- and 12-NO_2-CLA *versus* the corresponding β-products, which presented a different chromatographic profile (supplemental Fig. S2).

NO_2-CLA Reactions with HSA—Cys-34 in HSA is the most abundant reduced thiol in plasma and is therefore a potential target for reaction with NO_2-CLA. In addition, HSA has a central role in fatty acid binding and transport; therefore, both covalent and non-covalent interactions with NO_2-CLA might occur. The absorbance of NO_2-CLA changes with solvent polarity (λ_{max} 330 nm in aqueous solution *versus* 312 nm in methanol), and thus it is expected to also change upon interaction with the hydrophobic binding sites in HSA. NO_2-CLA incubation with delipidated thiol-blocked HSA resulted in a blue shift in absorbance (Fig. 9*A*). Titrations performed by adding aliquots of delipidated thiol-blocked HSA to a fixed amount of NO_2-CLA allowed us to estimate up to 3.8 ± 0.5 NO_2-CLA bound per delipidated thiol-blocked HSA (Fig. 9*B*). When titrations were carried out using lipidated (stearic acid/HSA, 5:1) thiol-blocked HSA, a similar value of 3.2 ± 0.2 NO_2-CLA per HSA was obtained indicating that NO_2-CLA was able to displace stearic acid (data not shown). Fitting of the titration data to hyperbolic equations yielded global apparent dissociation constants of $(0.9 \pm 0.3) \times 10^{-6}$ and $(1.2 \pm 0.3) \times 10^{-6}$ M for delipidated and lipidated HSA, respectively, consistent with reported values for non-nitroalkene fatty acids (46).

The reactivity of Cys-34 toward NO_2-CLA could not be evaluated following changes in absorbance at 330 nm because of interference from non-covalent binding. Therefore, the decay in HSA thiol concentration after incubation of reduced and lipidated HSA (50 μM) with NO_2-CLA (300 μM) for 1 h was assessed using 4,4′-dithiodipyridine (DTDP). The mole of thiol per mol of HSA were 0.47 and 0.25 in the absence and presence of NO_2-CLA, respectively. Considering the concentrations used and the incubation time, a lower limit of 0.5 M^{-1} s^{-1} (25 °C, pH 7.4) was estimated for the rate constant.

Discussion

NO_2-CLA reacts reversibly with thiols forming Michael adducts. In agreement with the presence of two electrophilic centers in NO_2-CLA, two products were detected, the β-adducts and the δ-adducts. The β-adducts are formed at faster rates and are thus the kinetic products. In contrast, the δ-adducts are formed with slower kinetics but present higher stabil-

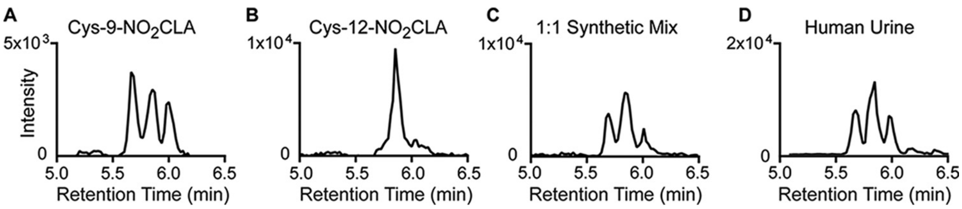

FIGURE 8. **LC-MS/MS profile of endogenous δ-Cys-NO_2-CLA addition products in human urine.** Comparison of isotopically labeled standards generated from the δ-addition of cysteine to 9-NO_2-CLA (*A*), 12-NO_2-CLA (*B*), a 1:1 mixture of both standards (*C*), and urine Cys-NO_2-CLA (*D*). Data were obtained from a single urine donor with LC-MS/MS profiles consistent with published reports (1, 2).

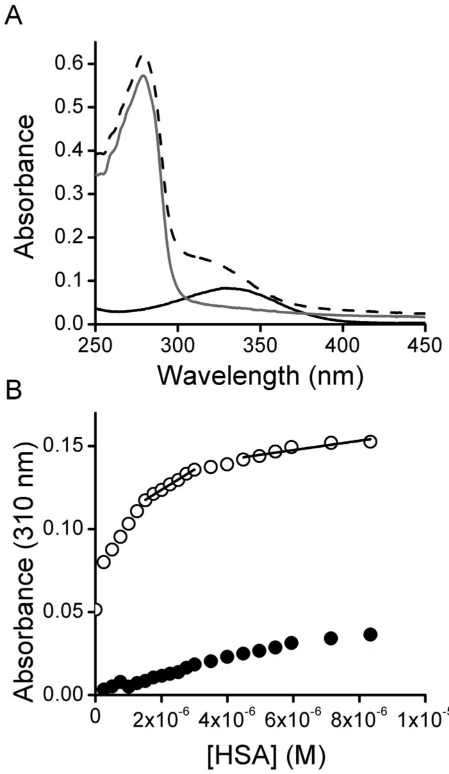

FIGURE 9. **NO_2-CLA binding to HSA.** *A,* UV-Visible spectra of 16 μM thiol-blocked delipidated HSA (*gray trace*), 10 μM NO_2-CLA (*black trace*), and the combination of both reagents (*dashed trace*). *B,* thiol-blocked delipidated HSA (0.2–10 μM) was mixed with NO_2-CLA (10 μM), and UV-visible spectra were recorded. The absorbance at 310 nm was plotted against HSA concentration, and the amount of NO_2-CLA bound was determined from the change in the slope (*open circles*). A control without NO_2-CLA was included (*black circles*).

ity and are thus the thermodynamic products. In the case of GSH, the δ-adduct is 30 times more stable than the β-adduct.

From a mechanistic viewpoint, our experimental and computational results are consistent with a stepwise addition process where the rate-controlling step involves the nucleophilic attack of the thiolate on NO_2-CLA to form an anionic intermediate, followed by proton incorporation, and the reverse process would be involved in elimination. Although nitroalkanes possess relatively high carbon acidity (pK_a 10.28 for nitromethane (43, 47)), deprotonation rates can be outstandingly slow, with rate constants for proton transfer from nitromethane to OH^- measured at 27.6 $M^{-1}\,s^{-1}$ (43, 47). In fact, deprotonation has been proposed to control the rate of elimination of other activated alkanes (25). However, in the case of the reaction between NO_2-CLA and thiols, the Brønsted correlations obtained together with the lack of a solvent deuterium kinetic isotopic effect rule out protonation as the rate-controlling step in the addition process (or deprotonation in the elimination).

The results obtained in this study can be generalized to predict the stability of NO_2-CLA adducts as a function of thiol pK_a. If specific aspects of protein thiol reactivity and steric constraints are dismissed, the K_{eq} at a certain pH can be calculated from dividing k_{off} and k_{on} and combining Equations 3–5 to obtain Equation 6.

$$\log K_{eq} = (\beta_{lg} - \beta_{nuc} + 1)pK_a + C_{off} - C_{on} + \log(K_a + [H^+]) \quad \text{(Eq. 6)}$$

For both the β- and the δ-adducts, substitution in Equation 6 with the β_{lg}, β_{nuc}, C_{off}, and C_{on} values obtained from Fig. 5 allows the generalization that, at pH 7.4, the stability of the adducts increases as the pK_a increases, so that adducts formed with relatively less acidic thiols (higher pK_a) are the more stable at neutral pH (Fig. 10).

Considering the wide variety of thiols present in the biological context and the reversibility of the reactions described herein, it is likely that NO_2-CLA will exist as part of a dynamic pool alternating between free and bound forms. Our study predicts that under intracellular conditions, NO_2-CLA will quickly react with GSH and other low and high molecular weight thiols to initially form β-adducts. Because of the reversibility of these reactions, the β-adducts will undergo elimination, and the free NO_2-CLA will eventually give rise to the more stable δ-adducts. Thus, the transient formation of β-adducts could contribute to establish a dynamic buffer of NO_2-CLA. Considering the high concentrations of GSH (2–17 mM) and protein thiols inside cells (10–50 mM) (18, 19), we can predict that if equilibrium is achieved >99% of the NO_2-CLA pool will correspond to covalently bound forms (assuming similar reactivity for protein thiols and free cysteine). Furthermore, <4% of these products will correspond to β-adducts and >96% to δ-adducts, given the higher stability of the latter. In plasma, considering the lower concentrations of thiols (~450 μM), it can be predicted that a significant fraction of the NO_2-CLA pool will be non-covalently bound to HSA, probably impacting its transport and storage. Nevertheless, it is important to understand that the interaction of NO_2-CLA with a particular protein thiol will be affected by the environment of the nucleophilic residue.

The adducts formed with GSH can be exported out of the cell through multi-drug resistance protein channels, which is a prominent pathway for nitroalkene fatty acid cell clearance. Once in the extracellular milieu, GSH-NO_2-CLA adducts are processed by γ-glutamyl transpeptidases and dipeptidases/aminopeptidases. The resulting cysteine conjugates are ex-

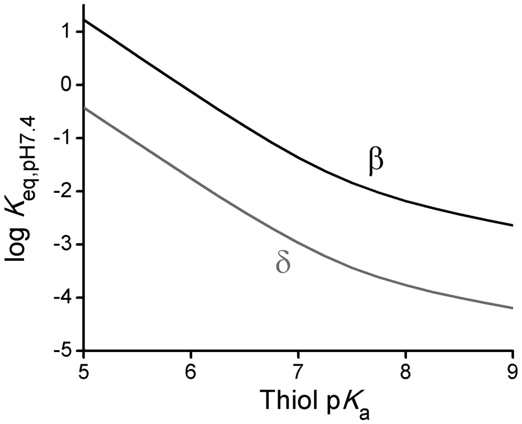

FIGURE 10. **Predicted stability of the adducts at pH 7.4 as a function of thiol pK_a.** The logarithm of the apparent dissociation equilibrium constant (K_{eq}) at pH 7.4 of β- (*black*) and δ- (*gray*) adducts was calculated from Eq. 6 using parameters obtained from Fig. 5.

creted in the urine. A small portion of the cysteine conjugates can be *N*-acetylated intracellularly forming mercapturic acid derivatives (2, 28, 48).

The finding of adducts of NO_2-CLA with cysteine in urine provides evidence for the *in vivo* reaction of NO_2-CLA with thiols. Moreover, it is likely that these adducts originated intracellularly by conjugation with GSH followed by cell export, removal of the glutamyl and glycyl moieties, and excretion. The fact that the Cys-NO_2-CLA adducts found in urine correspond to δ-addition products is consistent with the higher stability of the δ- *versus* β-adducts of cysteine and GSH.

Overall, we have performed an in-depth study of the interactions of NO_2-CLA with biological thiols and HSA. As the beneficial health effects of nitroalkene fatty acids continue to be unveiled, our study contributes to the understanding of the chemistry that underlies the protective actions of these endogenously formed potential drug candidates.

Experimental Procedures

General Solutions—All experiments were performed in 0.1 M phosphate buffer at pH 7.4, containing 0.1 mM DTPA unless otherwise specified. Low molecular weight thiol solutions were prepared in nanopure water and used on the same day. TNB was synthesized as described previously (49). Thiol concentrations were determined with DTNB before and after experiments using an absorption coefficient at 412 nm of 14,150 M^{-1} cm^{-1} (50). Stearic acid solutions (100 mM) were freshly prepared in methanol (80 °C, with agitation). DTDP solution (0.25 mM) was prepared in phosphate buffer, 0.1 M, pH 7.0.

Nitroalkene Fatty Acid and Adduct Solutions—10-Nitrooctadec-9-enoic acid (nitrooleic acid, NO_2-OA), 9- and 12-nitrooctadeca-9,11-dienoic acids (9- and 12-NO_2-CLA), or purified isomer solutions were synthesized as described (51, 52). For kinetic experiments, a 1:1 mixture of 9- and 12-NO_2-CLA or purified isomer solutions were prepared (2 mM in methanol) and kept at −80 °C until use. An absorption coefficient for NO_2-CLA at 330 nm in phosphate buffer of 6,490 M^{-1} cm^{-1} was determined based on the previously reported absorption coefficient at 312 nm in methanol (11,200 M^{-1} cm^{-1}) (52). The extinction coefficient used for NO_2-OA was 8,220 M^{-1} cm^{-1} at 270 nm in phosphate buffer (29). Isotopically labeled Cys-δ-adducts of 9- and 12-NO_2-CLA standards were synthesized by reacting an excess of $^{13}C_3$,^{15}N-Cys (500 μM) with either 9- or 12-NO_2-CLA (10 μM) for 60 min in 10 mM sodium phosphate buffer at pH 7.4, 25 °C. The reaction was stopped by 1:3 dilution in 10% formic acid, followed by addition of 7 volumes of methanol.

HSA Solutions—HSA was delipidated with activated charcoal as described (53). Reduced HSA was prepared by incubation with BME (10 mM, for 30 min at room temperature with agitation) followed by gel filtration on PD-10 columns equilibrated with phosphate buffer (0.1 M, pH 7.4, 0.1 mM DTPA). Thiol-blocked HSA was prepared by incubating delipidated HSA with BME followed by addition of NEM (150 mM, for 15 min at room temperature with agitation), followed by gel filtration against phosphate buffer. Lipidated and reduced HSA was prepared by incubating delipidated HSA with 5:1 stearic acid (stearic acid/HSA) (30 min at room temperature with agitation) followed by addition of BME and subsequent gel filtration. The HSA concentration was determined from the absorbance at 279 nm (ϵ = 0.531 $(g/liter)^{-1}$ cm^{-1}, 66,438 Da) (46). HSA thiols were measured with DTNB in sodium pyrophosphate buffer (0.1 M, pH 9, 5 min) (54).

UV-Visible Assessment of Nitroalkene Fatty Acid Reactions with Thiols—NO_2-CLA (10 μM) was reacted with GSH (0.2–15 mM), cysteine (Cys, 0.5–7 mM), homocysteine (0.5–12 mM), cysteinylglycine (1.5–7 mM), BME (1–8 mM), and TNB (60–100 μM). Changes in absorbance were followed at 330 nm (25 °C, pH 7.4). In some experiments, absorbance at 250, 290, or 412 (for TNB) nm, was also followed. For pH-dependence experiments, NO_2-CLA (10 μM) was mixed with GSH (1–4 mM) using buffers of constant ionic strength and varying pH values (100 mM MES, 52 mM Tris, and 52 mM ethanolamine) (55). The reaction of NO_2-OA (10 μM) with GSH (0.2–2 mM) was followed at 285 nm. Absorbance determinations were done in a Varian Cary 50 spectrophotometer equipped with an Applied Photophysics RX2000 Rapid Kinetics accessory.

Kinetics in Deuterium Oxide—For comparison of the kinetics of the reaction of NO_2-CLA with GSH in D_2O (Millipore, 92% final concentration) *versus* H_2O (50 mM phosphate buffer, pH 7.4), the fraction of ionized thiolate in D_2O was equaled to that in H_2O by calculating the pK_a in D_2O (56) and adjusting the pD. The value of pD was obtained by adding 0.4 to the measured pH.

Reactivity Patterns in 9-/12-NO_2-CLA as Explored by Electronic Structure Computational Modeling—Aqueous solution structures of 9-/12-NO_2-CLA were fully optimized and verified by inspection of the Hessian eigenvalues at the PCM(IEF)-ωB97X-D/6-31+G(d,p) level (57–59), including non-electrostatic contributions to solvation as implemented in Gaussian09 revision D.01 (60). Each solute was contained in a molecular shaped cavity constructed with Bondi's radii (61). ωB97X-D density functional was chosen based on its known superior performance in modeling thio-Michael additions (62). Energies of the highest occupied and lowest unoccupied Kohn-Sham orbitals (ϵ_{HOMO} and ϵ_{LUMO}, respectively) were used to assess global softness S as the inverse of the global chemical hardness η, calculated as follows:

$$S^{-1} = \eta = \epsilon_{LUMO} - \epsilon_{HOMO} \quad \text{(Eq. 7)}$$

The electrophilic Fukui function $f^+(r)$, measuring the propensity of NO_2-CLA to gain electron density in a nucleophilic attack, was also evaluated for each regioisomer within a finite difference approach (63), as shown in Equation 8,

$$f^+(r) = \rho_{N+1}(r) - \rho_N(r) \quad \text{(Eq. 8)}$$

where $\rho_N(r)$ and $\rho_{N+1}(r)$ represent the electron density at each point r around the molecule, respectively, obtained for NO_2-CLA in the anionic state of reference (N) and after gaining one extra electron at the ground-state geometry ($N + 1$) determined by single-point calculations at the same level of theory. Electrophilic sites were thus inspected by mapping $f^+(r)$ on a molecular surface of 0.0004 au isodensity by using Gaussview5 for generating the molecular graphics represented in Fig. 2 (64). To further assess differences among carbon electrophilic sites within each molecule, condensed Fukui function for each atom A (65) was also obtained by applying a Natural Bond Orbital (NBO) calculation and deriving NPA atomic charges q_A from the corresponding population analysis (66) as expressed in Equation 9,

$$f_A^+ = q_A^{N+1} - q_A^N \quad \text{(Eq. 9)}$$

Electrophilic atomic indices (condensed atomic softness, s_A^+) were finally obtained as shown in Equation 10,

$$s_A^+ = S \cdot f_A^+ \quad \text{(Eq. 10)}$$

Computational Modeling of the Detailed Mechanism of Thio-Michael Additions at C_β/C_δ Using Representative Model Species—Geometries of the RC, TS, and the anionic intermediate products (I) for the addition of methane thiolate at the C_β/C_δ positions of a representative conjugated nitro-olefin moiety (2-nitrohexa-2,4-diene) were fully optimized and verified at the same level of theory as previously applied for NO_2-CLA 9-/12-regioisomers. IRC reaction paths (67) correspondingly interconnecting them were generated with the HPC algorithm (68). Thermochemistry was calculated at 298 K and 1 atm under the usual statistical thermodynamics approaches (unscaled harmonic vibrational frequencies and rigid rotors) as implemented in Gaussian09 D.01 (60). NPA atomic charges (66) and WBIs (69) were also extracted from the corresponding electronic structures. The structure and relative stability of the tautomeric products further obtained after protonation of the anionic intermediate outcoming from each thiolate direct addition on C_β/C_δ were also characterized at the same level of theory, assessing the corresponding PA as Gibbs free-energy differences between the protonated and deprotonated form of each species. This approach has been recently validated by Taunton and co-workers (70) in an integrated kinetic and computational characterization of thio-Michael adducts established between activated acrylonitriles and β-mercaptoethanol. Molecular graphics representing the 3D structure of the species characterized were prepared with Discovery Studio Visualizer 4.0 (Accelrys). Molecular electrostatic potential was mapped for both nitronate intermediates on a total electronic density surface of 0.004 au, obtaining graphical representations with Gaussview5 (Semichem Inc.) (64).

LC-MS/MS Analysis of the Reaction between NO_2-CLA and β-Mercaptoethanol—9- or 12-NO_2-CLAs (10 μM) were reacted with BME (1.76 mM) in phosphate buffer, pH 7.4, at 25 °C. Aliquots were removed at different time points, and the reaction was stopped by dilution into 2 volumes of either 10% formic acid or 100 mM NEM. Samples were allowed to react for 30 min, diluted in 15 volumes of methanol, and subjected to LC-MS/MS analysis.

LC-MS/MS Analysis of NO_2-CLA-thiol Conjugates—NO_2-CLA and its conjugates were resolved by LC via reversed phase chromatography on an analytical C18 Luna column (2 × 100 mm, 5-μm particle size, Phenomenex) at a 0.65 ml/min flow rate using a water, 0.1% acetic acid (solvent A), and acetonitrile, 0.1% acetic acid (solvent B) solvent system. For BME-NO_2-CLA experiments, samples were loaded at 35% B for 0.3 min, and then % B was increased to 90% in 9.7 min. At 10 min the column was washed using 100% B for 2 min before equilibrating at 35% B for an additional 3 min. For urinary Cys-NO_2-CLA measurements, lipid extracts were loaded at 5% B for 0.5 min, and then the organic phase was increased to 35% over 3 min before being increased to 100% in 12 min. The column was washed for 3 min before re-equilibrating at 5% B for 2 min. MS analysis of BME-NO_2-CLA adducts was performed using an API Qtrap 4000 (Applied Biosystems, Framingham, MA) in the negative ion mode with the following settings: source temperature, 550 °C; curtain gas, 40; ionization spray voltage, −4500; GS1, 40; GS2, 40; declustering potential, −70 V; entrance potential, 4 V; collision energy, −17 and −35 V (BME conjugates and free NO_2-CLA respectively), and collision cell exit potential, −5 V. Analysis of urinary lipid extracts was performed using an API 5000 (Applied Biosystems) with the following settings: source temperature 650 °C; curtain gas, 50; ionization spray voltage, −4,500; GS1, 55; GS2, 50; declustering potential, −70 V; entrance potential, 4 V; collision energy, −20 and −35 V (cysteine conjugates and free NO_2-CLA respectively); collision cell exit potential, −5 V. The following transitions (m/z) were used: NO_2-CLA (324.3→46), BME-NO_2-CLA (402.3→324.3), Cys-NO_2-CLA (445.3→120), and $^{13}C_3{}^{15}N$ Cys-NO_2-CLA (449.3→124).

LC-UV-Visible Analysis of the Reaction between NO_2-CLA and BME—High performance liquid chromatography experiments were performed in an Agilent 1260 Infinity instrument. 9-NO_2-CLA (100 μM) was mixed with BME (1.76 mM) in phosphate buffer at 25 °C. At increasing times (10 s, 5 min, and 1 h), aliquots (70 μl) were mixed with 50% acetonitrile, 10% formic acid (140 μl). Samples (150 μl) were injected in a C18 column (Zorbax Eclipse Plus C18, 4.36 × 100 mm; 3.5 μm) and resolved using a linear gradient from 35 to 90% solution B in 19 min at a flow rate of 1 ml/min (solution B, acetonitrile, 0.1% acetic acid; solution A, H_2O, 0.1% acetic acid). The absorbance was registered using a diode array detector.

Determination of Non-covalent NO_2-CLA Binding to HSA—Increasing concentrations of thiol-blocked delipidated or lipidated HSA (0.2–10 μM) were mixed with NO_2-CLA (10 μM) in phosphate buffer, and the UV-Visible spectra were recorded. Control procedures were performed in the absence of NO_2-CLA.

Reaction between NO_2-CLA and HSA Thiol—Lipidated reduced HSA (50 μM) was mixed with NO_2-CLA (300 μM) or an equivalent volume of methanol (control) and incubated for 1 h (25 °C, pH 7.4). The samples were gel filtrated to remove excess NO_2-CLA, and protein concentration was determined using both absorbance measurements at 279 nm and the bicinchoninic acid assay (71). The remaining free thiols were quantified using DTDP (215 μM). Protein was first removed via ultrafiltration. Thiopyridone concentration was determined at 324 nm ($\epsilon = 21{,}400\ \text{M}^{-1}\ \text{cm}^{-1}$) (50) in the ultrafiltrate after baseline subtraction.

Nitroalkene Fatty Acid Extraction from Human Urine—Urine samples were collected from healthy human volunteers and used immediately (2) (University of Pittsburgh IRB PRO07110032). Briefly, C18 SEPAK columns were conditioned with 1 column volume of 100% methanol and equilibrated with 2 volumes of 10% methanol, and 5 ml of urine were loaded. Columns were then washed with 2 volumes of 10% methanol and dried under vacuum, and lipids eluted with 1 volume of methanol. The solvent was evaporated, and the samples were resuspended in 100 μl of methanol for LC-MS/MS analysis.

Data Processing—Data were plotted and analyzed using OriginPro 8.0 (OriginLab) or Prism 6 (GraphPad). Unless specified, results are expressed as the means ± S.E. of independent experiments.

Author Contributions—L. T. and D. A. V. prepared the manuscript, contributed to writing, designed, performed, and analyzed experiments. L. L. performed experiments. E. L. C. designed, performed, and analyzed (with the assistance of C. S. in characterizing 12/9-NO_2-CLA local softness) computational modeling and wrote the corresponding sections of the manuscript. M. N. M. designed and performed LC-UV-Visible experiments. S. R. S. contributed to LC-MS/MS method development. S. R. W. synthesized nitrated fatty acids. B. A. and F. J. S. contributed to the overall concept, experimental design, data interpretation, and manuscript preparation. All authors have given approval to the final version of the manuscript.

Acknowledgments—We are grateful to Jenner Bonanata for technical assistance and to Andrés Abella (Universidad de la República) for help with the mathematics of the kinetic analysis.

References

1. Delmastro-Greenwood, M., Hughan, K. S., Vitturi, D. A., Salvatore, S. R., Grimes, G., Potti, G., Shiva, S., Schopfer, F. J., Gladwin, M. T., Freeman, B. A., and Gelhaus Wendell, S. (2015) Nitrite and nitrate-dependent generation of anti-inflammatory fatty acid nitroalkenes. *Free Radic. Biol. Med.* **89,** 333–341
2. Salvatore, S. R., Vitturi, D. A., Baker, P. R., Bonacci, G., Koenitzer, J. R., Woodcock, S. R., Freeman, B. A., and Schopfer, F. J. (2013) Characterization and quantification of endogenous fatty acid nitroalkene metabolites in human urine. *J. Lipid Res.* **54,** 1998–2009
3. Vitturi, D. A., Minarrieta, L., Salvatore, S. R., Postlethwait, E. M., Fazzari, M., Ferrer-Sueta, G., Lancaster, J. R., Jr, Freeman, B. A., and Schopfer, F. J. (2015) Convergence of biological nitration and nitrosation via symmetrical nitrous anhydride. *Nat. Chem. Biol.* **11,** 504–510
4. Schopfer, F. J., Cipollina, C., and Freeman, B. A. (2011) Formation and signaling actions of electrophilic lipids. *Chem. Rev.* **111,** 5997–6021
5. Vitturi, D. A., Chen, C. S., Woodcock, S. R., Salvatore, S. R., Bonacci, G., Koenitzer, J. R., Stewart, N. A., Wakabayashi, N., Kensler, T. W., Freeman, B. A., and Schopfer, F. J. (2013) Modulation of nitro-fatty acid signaling: prostaglandin reductase-1 is a nitroalkene reductase. *J. Biol. Chem.* **288,** 25626–25637
6. Delmastro-Greenwood, M., Freeman, B. A., and Wendell, S. G. (2014) Redox-dependent anti-inflammatory signaling actions of unsaturated fatty acids. *Annu. Rev. Physiol.* **76,** 79–105
7. Kelley, E. E., Baust, J., Bonacci, G., Golin-Bisello, F., Devlin, J. E., St Croix, C. M., Watkins, S. C., Gor, S., Cantu-Medellin, N., Weidert, E. R., Frisbee, J. C., Gladwin, M. T., Champion, H. C., Freeman, B. A., and Khoo, N. K. (2014) Fatty acid nitroalkenes ameliorate glucose intolerance and pulmonary hypertension in high-fat diet-induced obesity. *Cardiovasc. Res.* **101,** 352–363
8. Liu, H., Jia, Z., Jia, Z., Soodvilai, S., Guan, G., Wang, M. H., Dong, Z., Symons, J. D., and Yang, T. (2008) Nitro-oleic acid protects the mouse kidney from ischemia and reperfusion injury. *Am. J. Physiol. Renal Physiol.* **295,** F942–F949
9. Rudolph, T. K., Rudolph, V., Edreira, M. M., Cole, M. P., Bonacci, G., Schopfer, F. J., Woodcock, S. R., Franek, A., Pekarova, M., Khoo, N. K., Hasty, A. H., Baldus, S., and Freeman, B. A. (2010) Nitro-fatty acids reduce atherosclerosis in apolipoprotein E-deficient mice. *Arterioscler. Thromb. Vasc. Biol.* **30,** 938–945
10. Rudolph, V., Rudolph, T. K., Schopfer, F. J., Bonacci, G., Woodcock, S. R., Cole, M. P., Baker, P. R., Ramani, R., and Freeman, B. A. (2010) Endogenous generation and protective effects of nitro-fatty acids in a murine model of focal cardiac ischaemia and reperfusion. *Cardiovasc. Res.* **85,** 155–166
11. Schopfer, F. J., Cole, M. P., Groeger, A. L., Chen, C. S., Khoo, N. K., Woodcock, S. R., Golin-Bisello, F., Motanya, U. N., Li, Y., Zhang, J., Garcia-Barrio, M. T., Rudolph, T. K., Rudolph, V., Bonacci, G., Baker, P. R., *et al.* (2010) Covalent peroxisome proliferator-activated receptor γ adduction by nitro-fatty acids: selective ligand activity and anti-diabetic signaling actions. *J. Biol. Chem.* **285,** 12321–12333
12. Villacorta, L., Chang, L., Salvatore, S. R., Ichikawa, T., Zhang, J., Petrovic-Djergovic, D., Jia, L., Carlsen, H., Schopfer, F. J., Freeman, B. A., and Chen, Y. E. (2013) Electrophilic nitro-fatty acids inhibit vascular inflammation by disrupting LPS-dependent TLR4 signalling in lipid rafts. *Cardiovasc. Res.* **98,** 116–124
13. Wang, H., Liu, H., Jia, Z., Jia, Z., Olsen, C., Litwin, S., Guan, G., and Yang, T. (2010) Nitro-oleic acid protects against endotoxin-induced endotoxemia and multiorgan injury in mice. *Am. J. Physiol. Renal Physiol.* **298,** F754–F762
14. Charles, R. L., Rudyk, O., Prysyazhna, O., Kamynina, A., Yang, J., Morisseau, C., Hammock, B. D., Freeman, B. A., and Eaton, P. (2014) Protection from hypertension in mice by the Mediterranean diet is mediated by nitro fatty acid inhibition of soluble epoxide hydrolase. *Proc. Natl. Acad. Sci. U.S.A.* **111,** 8167–8172
15. Fazzari, M., Trostchansky, A., Schopfer, F. J., Salvatore, S. R., Sánchez-Calvo, B., Vitturi, D., Valderrama, R., Barroso, J. B., Radi, R., Freeman, B. A., and Rubbo, H. (2014) Olives and olive oil are sources of electrophilic fatty acid nitroalkenes. *PLoS ONE* **9,** e84884
16. Fox, R. J., Miller, D. H., Phillips, J. T., Hutchinson, M., Havrdova, E., Kita, M., Yang, M., Raghupathi, K., Novas, M., Sweetser, M. T., Viglietta, V., Dawson, K. T., and CONFIRM Study Investigators (2012) Placebo-controlled phase 3 study of oral BG-12 or glatiramer in multiple sclerosis. *N. Engl. J. Med.* **367,** 1087–1097
17. Gold, R., Kappos, L., Arnold, D. L., Bar-Or, A., Giovannoni, G., Selmaj, K., Tornatore, C., Sweetser, M. T., Yang, M., Sheikh, S. I., Dawson, K. T., and DEFINE Study Investigators (2012) Placebo-controlled phase 3 study of oral BG-12 for relapsing multiple sclerosis. *N. Engl. J. Med.* **367,** 1098–1107
18. Hansen, R. E., Roth, D., and Winther, J. R. (2009) Quantifying the global cellular thiol-disulfide status. *Proc. Natl. Acad. Sci. U.S.A.* **106,** 422–427
19. Requejo, R., Hurd, T. R., Costa, N. J., and Murphy, M. P. (2010) Cysteine residues exposed on protein surfaces are the dominant intramitochondrial thiol and may protect against oxidative damage. *FEBS J.* **277,** 1465–1480

20. Gutscher, M., Pauleau, A. L., Marty, L., Brach, T., Wabnitz, G. H., Samstag, Y., Meyer, A. J., and Dick, T. P. (2008) Real-time imaging of the intracellular glutathione redox potential. *Nat. Methods* **5,** 553–559
21. Østergaard, H., Tachibana, C., and Winther, J. R. (2004) Monitoring disulfide bond formation in the eukaryotic cytosol. *J. Cell Biol.* **166,** 337–345
22. Turell, L., Radi, R., and Alvarez, B. (2013) The thiol pool in human plasma: the central contribution of albumin to redox processes. *Free Radic. Biol. Med.* **65,** 244–253
23. Bernasconi, C. F., and Killion, R. B. (1988) High intrinsic rate constant and large imbalances in the thiolate ion addition to substituted *a*-nitrostilbenes. *J. Am. Chem. Soc.* **110,** 7506–7512
24. Cann, P. F., and Stirling, C. J. (1974) Elimination and addition reactions. Part XXIII. Mechanisms of elimination in nitro-compounds bearing phenoxy and phenyltio leaving groups. *J. Chem. Soc. Perkin Trans. 2,* 820–823
25. Fishbein, J. C., and Jencks, W. P. (1988) Elimination reactions of *b*-cyano thioethers. Evidence for a carbanion intermediate and a change in rate-limiting step. *J. Am. Chem. Soc.* **110,** 5075–5086
26. Friedman, M., Cavins, J. F., and Wall, J. S. (1965) Relative nucleophilic reactivities of amino groups and mercaptide ions in addition reactions with *a, b*-unsaturated compounds. *J. Am. Chem. Soc.* **87,** 3672–3682
27. Bonacci, G., Baker, P. R., Salvatore, S. R., Shores, D., Khoo, N. K., Koenitzer, J. R., Vitturi, D. A., Woodcock, S. R., Golin-Bisello, F., Cole, M. P., Watkins, S., St Croix, C., Batthyany, C. I., Freeman, B. A., and Schopfer, F. J. (2012) Conjugated linoleic acid is a preferential substrate for fatty acid nitration. *J. Biol. Chem.* **287,** 44071–44082
28. Alexander, R. L., Bates, D. J., Wright, M. W., King, S. B., and Morrow, C. S. (2006) Modulation of nitrated lipid signaling by multidrug resistance protein 1 (MRP1): glutathione conjugation and MRP1-mediated efflux inhibit nitrolinoleic acid-induced, PPARγ-dependent transcription activation. *Biochemistry* **45,** 7889–7896
29. Baker, L. M., Baker, P. R., Golin-Bisello, F., Schopfer, F. J., Fink, M., Woodcock, S. R., Branchaud, B. P., Radi, R., and Freeman, B. A. (2007) Nitro-fatty acid reaction with glutathione and cysteine. Kinetic analysis of thiol alkylation by a Michael addition reaction. *J. Biol. Chem.* **282,** 31085–31093
30. Fersht, A. (1999) *Structure and Mechanism in Protein Science: A Guide to Enzyme Catalysis and Protein Folding*, pp. 150–153, W. H. Freeman & Co., New York
31. Fierke, C. A., and Hammes, G. G. (1995) Transient kinetic approaches to enzyme mechanisms. *Methods Enzymol.* **249,** 3–37
32. Baker, P. R., Lin, Y., Schopfer, F. J., Woodcock, S. R., Groeger, A. L., Batthyany, C., Sweeney, S., Long, M. H., Iles, K. E., Baker, L. M., Branchaud, B. P., Chen, Y. E., and Freeman, B. A. (2005) Fatty acid transduction of nitric oxide signaling: multiple nitrated unsaturated fatty acid derivatives exist in human blood and urine and serve as endogenous peroxisome proliferator-activated receptor ligands. *J. Biol. Chem.* **280,** 42464–42475
33. Schopfer, F. J., Batthyany, C., Baker, P. R., Bonacci, G., Cole, M. P., Rudolph, V., Groeger, A. L., Rudolph, T. K., Nadtochiy, S., Brookes, P. S., and Freeman, B. A. (2009) Detection and quantification of protein adduction by electrophilic fatty acids: mitochondrial generation of fatty acid nitroalkene derivatives. *Free Radic. Biol. Med.* **46,** 1250–1259
34. Rudolph, V., Schopfer, F. J., Khoo, N. K., Rudolph, T. K., Cole, M. P., Woodcock, S. R., Bonacci, G., Groeger, A. L., Golin-Bisello, F., Chen, C. S., Baker, P. R., and Freeman, B. A. (2009) Nitro-fatty acid metabolome: saturation, desaturation, β-oxidation, and protein adduction. *J. Biol. Chem.* **284,** 1461–1473
35. Bednar, R. A. (1990) Reactivity and pH dependence of thiol conjugation to *N*-ethylmaleimide: detection of a conformational change in chalcone isomerase. *Biochemistry* **29,** 3684–3690
36. Portillo-Ledesma, S., Sardi, F., Manta, B., Tourn, M. V., Clippe, A., Knoops, B., Alvarez, B., Coitiño, E. L., and Ferrer-Sueta, G. (2014) Deconstructing the catalytic efficiency of peroxiredoxin-5 peroxidatic cysteine. *Biochemistry* **53,** 6113–6125
37. Espenson, J. H. (1995) *Chemical Kinetics and Reaction Mechanisms*, 2nd Ed., pp. 142–145, McGraw Hill, Inc., New York
38. Mulliner, D., Wondrousch, D., and Schüürmann, G. (2011) Predicting Michael-acceptor reactivity and toxicity through quantum chemical transition-state calculations. *Org. Biomol. Chem.* **9,** 8400–8412
39. Thomas, B. E., and Kollman, P. A. (1995) An *ab initio* molecular orbital study of the first step of the catalytic mechanism of thymidylate synthase: the Michael addition of sulfur and oxygen nucleophiles. *J. Org. Chem.* **60,** 8375–8381
40. Krenske, E. H., Petter, R. C., Zhu, Z., and Houk, K. N. (2011) Transition states and energetics of nucleophilic additions of thiols to substituted α,β-unsaturated ketones: substituent effects involve enone stabilization, product branching, and solvation. *J. Org. Chem.* **76,** 5074–5081
41. Bernasconi, C. F. (1991) in *Advances in Physical Organic Chemistry* (Bethell, D., ed) pp. 119–238, Academic Press
42. Ando, K., Shimazu, Y., Seki, N., and Yamataka, H. (2011) Kinetic study of proton-transfer reactions of phenylnitromethanes. Implication for the origin of nitroalkane anomaly. *J. Org. Chem.* **76,** 3937–3945
43. Bernasconi, C. F., Kliner, D. A. V., Mullin, A. S., and Ni, J. X. (1988) Kinetics of ionization of nitromethane and phenylnitromethane by amines and carboxylate ions in Me_2SO water mixtures– evidence of ammonium ion nitronate ion hydrogen-bonded complex-formation in Me_2SO-rich solvent mixtures. *J. Org. Chem.* **53,** 3342–3351
44. Moutiers, G., Thuet, V., and Terrier, F. (1997) The nitroalkane behaviour of (4-nitrophenyl)nitromethane: a kinetic and structural study in H_2O-Me_2SO mixtures. *J. Chem. Soc. Perkin Trans.* **2,** 1479–1486
45. Sato, M., Kitamura, Y., Yoshimura, N., and Yamataka, H. (2009) Proton-transfer reactions of nitroalkanes: the role of aci-nitro species. *J. Org. Chem.* **74,** 1268–1274
46. Peters, T. (1996) *All About Albumin. Biochemistry, Genetics and Medical Applications*, pp. 79–95, Academic Press, San Diego
47. Bell, R. P., and Goodall, D. M. (1966) Kinetic hydrogen isotope effects in the ionization of some nitroparaffins. *Proc. R. Soc. Lond. A Math. Phys. Sci.* **294,** 273–297
48. Ramsay, E. E., and Dilda, P. J. (2014) Glutathione *S*-conjugates as prodrugs to target drug-resistant tumors. *Front. Pharmacol.* **5,** 181
49. Turell, L., Botti, H., Carballal, S., Ferrer-Sueta, G., Souza, J. M., Durán, R., Freeman, B. A., Radi, R., and Alvarez, B. (2008) Reactivity of sulfenic acid in human serum albumin. *Biochemistry* **47,** 358–367
50. Riener, C. K., Kada, G., and Gruber, H. J. (2002) Quick measurement of protein sulfhydryls with Ellman's reagent and with 4,4′-dithiodipyridine. *Anal. Bioanal. Chem.* **373,** 266–276
51. Woodcock, S. R., Bonacci, G., Gelhaus, S. L., and Schopfer, F. J. (2013) Nitrated fatty acids: synthesis and measurement. *Free Radic. Biol. Med.* **59,** 14–26
52. Woodcock, S. R., Salvatore, S. R., Bonacci, G., Schopfer, F. J., and Freeman, B. A. (2014) Biomimetic nitration of conjugated linoleic acid: formation and characterization of naturally occurring conjugated nitrodienes. *J. Org. Chem.* **79,** 25–33
53. Chen, R. F. (1967) Removal of fatty acids from serum albumin by charcoal treatment. *J. Biol. Chem.* **242,** 173–181
54. Alvarez, B., Carballal, S., Turell, L., and Radi, R. (2010) Formation and reactions of sulfenic acid in human serum albumin. *Methods Enzymol.* **473,** 117–136
55. Ellis, K. J., and Morrison, J. F. (1982) Buffers of constant ionic strength for studying pH-dependent processes. *Methods Enzymol.* **87,** 405–426
56. Jencks, W. P., and Salvesen, K. (1971) Equilibrium deuterium isotope effects on the ionization of thiol acids. *J. Am. Chem. Soc.* **93,** 4433–4436
57. Chai, J. D., and Head-Gordon, M. (2008) Long-range corrected hybrid density functionals with damped atom-atom dispersion corrections. *Phys. Chem. Chem. Phys.* **10,** 6615–6620
58. Ditchfield, R., Hehre, W. J., and Pople, J. A. (1971) Self-consistent molecular-orbital methods. IX. An extended Gaussian-type basis for molecular-orbital studies of organic molecules. *J. Chem. Phys.* **54,** 724–728
59. Tomasi, J. (2011) Selected features of the polarizable continuum model for the representation of solvation. *Wiley Int. Rev. Comput. Mol. Sci.* **1,** 855–867
60. Frisch, M. J., Trucks, G. W., Schlegel, H. B., Scuseria, G. E., Robb, M. A., Cheeseman, J. R., Scalmani, G., Barone, V., Mennucci, B., Petersson, G. A., Nakatsuji, H., Caricato, M., Li, X., Hratchian, H. P., Izmaylov,

A. F., *et al.* (2013) *Gaussian 09,* Revision D.01 Ed., Gaussian, Inc., Wallingford, CT

61. Bondi, A. (1964) van der Waals volumes and radii. *J. Phys. Chem.* **68,** 441–451
62. Smith, J. M., Jami Alahmadi, Y., and Rowley, C. N. (2013) Range-separated DFT functionals are necessary to model Thio-Michael additions. *J. Chem. Theory Comput.* **9,** 4860–4865
63. Geerlings, P., De Proft, F., and Langenaeker, W. (2003) Conceptual density functional theory. *Chem. Rev.* **103,** 1793–1873
64. Dennington, R., Keith, T., and Millam, J. (2009) *GaussView,* Version 5, Semichem Inc., Shawnee Mission, KS
65. Yang, W., and Mortier, W. J. (1986) The use of global and local molecular parameters for the analysis of the gas-phase basicity of amines. *J. Am. Chem. Soc.* **108,** 5708–5711
66. Glendening, E. D., Landis, C. R., and Weinhold, F. (2012) Natural bond orbital methods. *Wires Comput. Mol. Sci.* **2,** 1–42
67. Fukui, K. (1981) The path of chemical reactions–the IRC approach. *Acc. Chem. Res.* **14,** 363–368
68. Hratchian, H. P., and Schlegel, H. B. (2005) Using Hessian updating to increase the efficiency of a Hessian based predictor-corrector reaction path following method. *J. Chem. Theory Comput.* **1,** 61–69
69. Wiberg, K. B. (1968) Application of the Pople-Santry-Segal CNDO method to the cyclopropylcarbinyl and cyclobutyl cation and to bicyclobutane. *Tetrahedron* **24,** 1083–1096
70. Krishnan, S., Miller, R. M., Tian, B., Mullins, R. D., Jacobson, M. P., and Taunton, J. (2014) Design of reversible, cysteine-targeted Michael acceptors guided by kinetic and computational analysis. *J. Am. Chem. Soc.* **136,** 12624–12630
71. Smith, P. K., Krohn, R. I., Hermanson, G. T., Mallia, A. K., Gartner, F. H., Provenzano, M. D., Fujimoto, E. K., Goeke, N. M., Olson, B. J., and Klenk, D. C. (1985) Measurement of protein using bicinchoninic acid. *Anal. Biochem.* **150,** 76–85